JACS
JOURNAL OF THE AMERICAN CHEMICAL SOCIETY

Article

pubs.acs.org/JACS

Long-Cycling Aqueous Organic Redox Flow Battery (AORFB) toward Sustainable and Safe Energy Storage

Bo Hu, Camden DeBruler, Zayn Rhodes, and T. Leo Liu*

The Department of Chemistry and Biochemistry, Utah State University, Logan, Utah 84322-1400, United States

Supporting Information

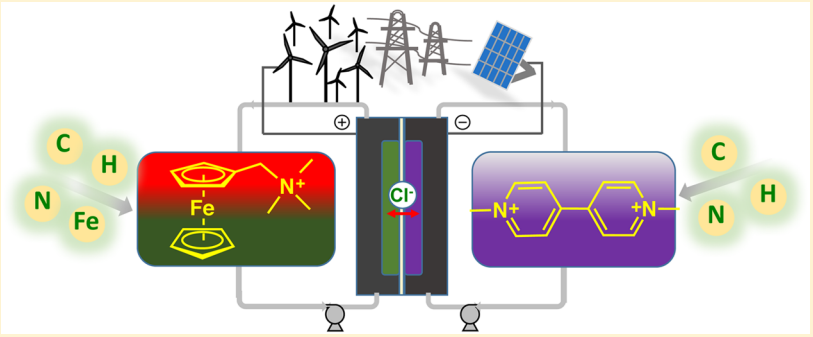

ABSTRACT: Redox flow batteries (RFBs) are a viable technology to store renewable energy in the form of electricity that can be supplied to electricity grids. However, widespread implementation of traditional RFBs, such as vanadium and Zn−Br_2 RFBs, is limited due to a number of challenges related to materials, including low abundance and high costs of redox-active metals, expensive separators, active material crossover, and corrosive and hazardous electrolytes. To address these challenges, we demonstrate a neutral aqueous organic redox flow battery (AORFB) technology utilizing a newly designed cathode electrolyte containing a highly water-soluble ferrocene molecule. Specifically, water-soluble (ferrocenylmethyl)trimethylammonium chloride (**FcNCl**, 4.0 M in H_2O, 107.2 Ah/L, and 3.0 M in 2.0 NaCl, 80.4 Ah/L) and N^1-ferrocenylmethyl-N^1,N^1,N^2,N^2,N^2-pentamethylpropane-1,2-diaminium dibromide, (**FcN_2Br_2**, 3.1 M in H_2O, 83.1 Ah/L, and 2.0 M in 2.0 M NaCl, 53.5 Ah/L) were synthesized through structural decoration of hydrophobic ferrocene with synergetic hydrophilic functionalities including an ammonium cation group and a halide anion. When paired with methyl viologen (**MV**) as an anolyte, resulting **FcNCl**/**MV** and **FcN_2Br_2**/**MV** AORFBs were operated in noncorrosive neutral NaCl supporting electrolytes using a low-cost anion-exchange membrane. These ferrocene/**MV** AORFBs are characterized as having high theoretical energy density (45.5 Wh/L) and excellent cycling performance from 40 to 100 mA/cm^2. Notably, the **FcNCl**/**MV** AORFBs (demonstrated at 7.0 and 9.9 Wh/L) exhibited unprecedented long cycling performance, 700 cycles at 60 mA/cm^2 with 99.99% capacity retention per cycle, and delivered power density up to 125 mW/cm^2. These AORFBs are built from earth-abundant elements and are environmentally benign, thus representing a promising choice for sustainable and safe energy storage.

INTRODUCTION

The increasing worldwide energy demand necessitates large-scale and efficient utilization of renewable energy, such as solar, wind, and hydroelectric power.[1] Simultaneously, the utilization of renewable energy can address environmental challenges instigated by the production and burning of fossil fuels. However, the intermittent and fluctuating nature of these renewable energy resources has to be mitigated using effective energy storage solutions.[1−3] Redox flow batteries (RFBs) have been recognized as a viable technology for large-scale energy storage (up to MW/MWh) by government agencies, industrial partners, and research institutions.[2−6] Compared to static rechargeable batteries (e.g., lead acid batteries and Li ion batteries), several technical merits enable RFBs to be well suited for integration of renewable energy and balancing electricity grids: high power input and output, decoupled energy and power, safety features, and scalability (up to MW/MWh).[2−4] Traditional inorganic RFBs, including vanadium RFBs and Zn−Br_2 RFBs, have evolved as relatively established technologies. However, their extensive applications for large-scale energy storage suffer from several major techno-economical drawbacks,[2−6] expensive and resource-limited active materials (vanadium RFBs), corrosive and hazardous electrolytes in both RFBs, low current performance (Zn−Br_2 RFBs due to Zn dendrite formation), electrolyte crossover, and expensive system costs, such as the Nafion membrane used in both RFBs. Thus, there is an urgent call to develop low-cost and safe RFB technologies to meet the burgeoning energy storage demands.

To address the challenges encountered by existing inorganic RFBs, we and others have proposed aqueous organic RFBs

Received: October 25, 2016
Published: December 14, 2016

DOI: 10.1021/jacs.6b10984
J. Am. Chem. Soc. 2017, 139, 1207−1214

(AORFBs) employing sustainable and abundant redox-active organic molecules as a new generation of RFBs for green energy storage.[7−14] In addition to the general features of RFBs discussed above, AORFBs have several outstanding advantages for large-scale energy storage: (1) using organic redox-active materials consisting of earth-abundant elements is a sustainable practice, and they are also synthetically tunable to gain high oxidation/reduction redox potentials and high solubility, thus high energy density RFBs; (2) utilization of nonflammable aqueous electrolytes offers safety benefits; (3) aqueous electrolytes consisting of water and simple inorganic supporting electrolytes such as NaCl and KOH are inexpensive; (4) high-conductivity aqueous electrolytes and well-developed selective ion-conductive membranes for aqueous electrolytes allow high power operation while achieving high energy efficiency. Specifically, we have been focusing on developing neutral aqueous organic RFBs for safe and low-cost large-scale and residential energy storage using sustainable, noncorrosive, and nonflammable aqueous redox-active electrolytes and low-cost ion-exchange membranes.[12] Several groups including our group have made significant progress in the emerging AORFB technology in the past few years, such as high-power acid/alkaline AORFBs[7−11,14] and high-voltage and low-cost neutral AORFBs.[12,13,15] Meanwhile, progress has also been made in developing nonaqueous organic RFBs (NAORFBs).[16−23]

However, in spite of the rapid advances, most of the reported AORFBs and NAORFBs only displayed limited cycling performance (typically not more than 100 cycles), which is primarily attributed to electrochemical and chemical instability of electrolyte materials. In addition, most of the reported AORFBs still have lower energy densities than the state of the art vanadium RFBs (41.8 Wh/L), which is limited by either catholyte or anolyte. We believe that these limitations can be mitigated by designing robust and high-capacity redox-active electrolyte materials. Herein we introduce a stable cycling AORFB technology named ferrocene/**MV** AORFBs (Figure 1). This redox flow battery technology is constructed on newly designed catholytes containing a highly soluble redox-active ferrocene compound, (ferrocenylmethyl)trimethylammonium chloride (**FcNCl**, 107.2 Ah/L in water and 80.4 Ah/L in 2.0 M NaCl) or N^1-ferrocenylmethyl-N^1,N^1,N^2,N^2,N^2-pentamethylpropane-1,2-diaminium dibromide (**FcN_2Br_2**, 83.1 Ah/L in water and 53.6 Ah/L in 2.0 M NaCl), along with methyl viologen (**MV**) anolyte, a neutral NaCl supporting electrolyte and a low-cost anion-exchange membrane. This is the first application of ferrocene compounds in AORFBs. These ferrocene/**MV** AORFBs are characterized by high theoretical energy density (up to 45.5 Wh/L) and excellent cycling performance from 40 to 100 mA/cm^2. In particular, the prototype **FcNCl**/**MV** AORFB (demonstrated at 7.0 and 9.9 Wh/L) exhibited unprecedented cycling performance, 700 cycles at 60 mA/cm^2 with 99.99% capacity retention per cycle, and up to 125 mW/cm^2 power density output in neutral electrolytes. The presented results highlight the great promise of AORFBs for energy storage applications.

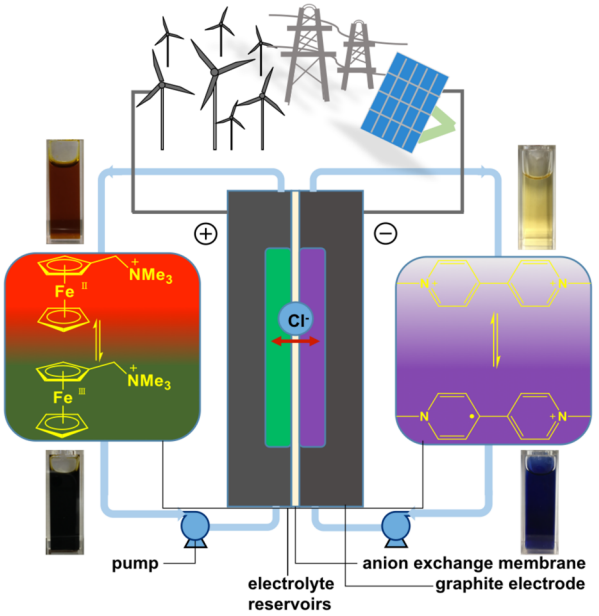

Figure 1. Schematic representation of the **FcNCl**/**MV** AORFB and illustrations of discharged and charged states of **FcNCl** and **MV** and cell reactions.

RESULTS AND DISCUSSION

Because of their reversible $Fe^{3+/2+}$ redox couple and thermal stability, the 1973 Nobel Prize winning organometallic complex, ferrocene, and its derivatives have been utilized in a wide array of applications in chemistry and materials science since their discovery in the 1950s.[24−26] In addition, synthesis of ferrocene derivatives has been well developed, involving low-cost starting materials based on earth-abundant elements: C, H, N, and Fe. Thus, they are sustainable and can be low cost in large-scale production. However, most of the known ferrocene compounds are aliphatic or hydrophobic, i.e., only soluble in organic solvents. Thus, ferrocene compounds have been only applied as the cathode in a couple of semiflow[21] or static liquid[27] Li/ferrocene nonaqueous batteries.

We rationalized that ferrocene compounds functionalized with hydrophilic groups could be water soluble and demonstrate superior performance in aqueous RFBs. Obviously, we first screened commercially available ferrocene compounds functionalized with hydrophilic functional groups (ferrocenecarboxylic acid, 1,1′-ferrocenedicarboxylic acid, and 1,1′-ferrocenedimethanol). However, these ferrocene derivatives are only slightly soluble in water, <100 mM, and therefore not suitable for applications in aqueous RFBs. We found that (ferrocenylmethyl)trialkylammonium iodides exhibited solubility in aqueous solutions,[28,29] although (ferrocenylmethyl)-dimethylethylammonium bis(trifluoromethane) sulfonimide (TFSI, a hydrophobic anion) applied in the nonaqueous Li/ferrocene RFB was reported nearly insoluble in water.[21] To apply the (ferrocenylmethyl)trialkylammonium redox-active moiety for ARFBs using selective Cl^- anion transfer mechanism, we are particularly interested in the (ferrocenylmethyl)trialkylammonium chloride redox-active species. In addition, compared to I^- (0.55 V vs NHE), Cl^- counterion has a much higher oxidation potential (1.40 V vs NHE) and will not interfere with the $Fe^{3+/2+}$ redox couple of the (ferrocenylmethyl)trialkylammonium moiety. Following the synthesis of (ferrocenylmethyl)trialkylammonium iodides,[28,29] we prepared (ferrocenylmethyl)trimethylammonium choride (**FcNCl**) through direct alkylation of (ferrocenylmethyl)-dimethylamine (**FcN**) with CH_3Cl. Simply mixing of (ferrocenylmethyl)dimethylamine with CH_3Cl in CH_3CN at room temperature (RT) resulted in the formation of red-orange **FcNCl** precipitates with a 95% isolated yield (Scheme 1). The one-step N-alkylation reaction is quite straightforward

DOI: 10.1021/jacs.6b10984
J. Am. Chem. Soc. 2017, 139, 1207−1214

Scheme 1

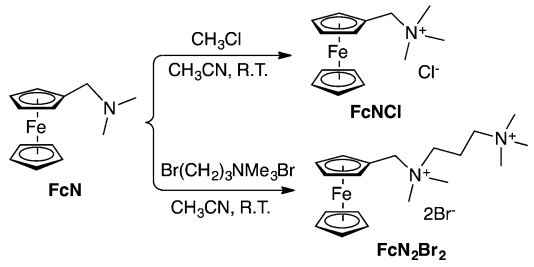

and was demonstrated at 20 g scale. **FcNCl** was fully characterized by ^{1}H NMR, UV−vis, and elemental analysis to establish its identity and purity (see Supporting Information).

FcNCl is surprisingly highly soluble in H_2O with a solubility of ca. 4.0 M, corresponding to a capacity 107.2 Ah/L, a desired characteristic for RFB applications. Even in 2.0 M NaCl, the solubility of **FcNCl** was recorded at 3.0 M (80.4 Ah/L). The high water solubility of **FcNCl** stimulated us to synthesize N^1-ferrocenylmethyl-N^1,N^1,N^2,N^2,N^2-pentamethylpropane-1,2-diaminium dibromide, **FcN_2Br_2** (Scheme 1), featuring two pendent ammonium groups. **FcN_2Br_2** exhibits a solubility of 3.1 M (83.1 Ah/L) in water and 2.0 M (53.6 Ah/L) in 2.0 M NaCl. The solubility and charge capacity of **FcNCl** and **FcN_2Br_2** are summarized in Table 1. In contrast, pristine ferrocene (Cp_2Fe) and the precursor, (ferrocenylmethyl)-dimethylamine, are insoluble or barely soluble in water. In addition, as stated above, (ferrocenylmethyl)dimethylethyl-ammonium TFSI is also insoluble in water.[21] It is believed that such high solubility of **FcNCl** and **FcN_2Br_2** is credited to the synergetic effects of their hydrophilic pendant ammonium functionality and halide counterion.

Cyclic voltammetry studies revealed a reversible $Fe^{3+/2+}$ redox couple at 0.61 V vs NHE for both **FcNCl** and **FcN_2Br_2** (Figure 2), indicating that the two ammonium substituents have nearly identical electronic influences on the ferrocene moiety. The pendent electron-withdrawing ammonium group of both compounds positively shifts the $Fe^{3+/2+}$ redox potential by 210 mV compared to the **FcN** precursor (0.40 V vs NHE for $Fe^{3+/2+}$). Considering the high capacities of these functionalized ferrocene compounds, their oxidation potentials are positive enough for AORFB applications. Scan rate dependence studies of **FcNCl** and **FcN_2Br_2** (Figure S1−S4) demonstrated that their reversible oxidation is a diffusion-controlled process.

To further understand the electrochemical kinetics of **FcNCl** and **FcN_2Br_2**, they were studied by linear sweep voltammetry (LSV) using a glassy carbon rotation disc electrode. The results are presented in Figures 3 and S5. The rotation speed was increased from 300 to 2400 rpm to gain different mass-transport-limited current with a scan rate at 5 mV/s (Figure 3A). The diffusion coefficient (D) of **FcNCl** was calculated to be 3.74×10^{-6} cm^2/s from the slope of the Levich plot using Levich equation (eq 1 given in the Experimental Section).

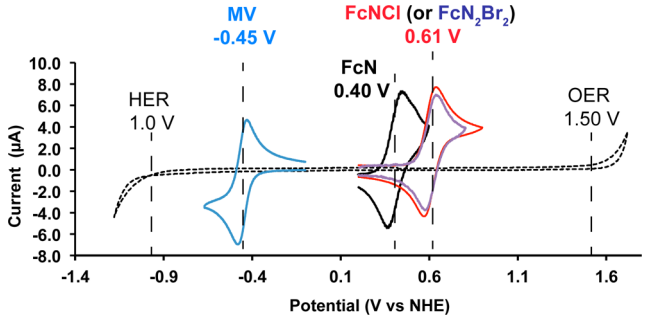

Figure 2. Cyclic voltammograms of **FcNCl** (red trace), **$FcNBr_2$** (purple trace), **FcN** (black trace), and **MV** (blue trace). Dashed curve is the cyclic voltammogram of 0.5 M NaCl, labeled with the onset potentials for hydrogen evolution reaction (HER, −1.00 V) and oxygen evolution reaction (OER, 1.50 V).

Subsequently, a plot of oxidation overpotential over the logarithm of the kinetic current (Figure 3C) was constructed to determine the rate constant (k^0) for the charge transfer process for the oxidation of **FcNCl**. The Tafel equation (eq 2 given in the Experimental Section) is applicable over 45 mV overpotential, and the fitted Tafel plot (shown as the blue dotted line in Figure 3C) yielded a rate constant of 3.66×10^{-5} cm/s for **FcNCl**. These same analyses (Figure S5) yielded a diffusion constant of 3.64×10^{-6} cm^2/s and an electron transfer rate constant of 4.60×10^{-6} cm/s for **FcN_2Br_2**. Large electron transfer rate and diffusion constants can contribute to reduced polarization overpotential due to the charge transfer and mass transport resistances. The electron transfer rate and diffusion constants of **FcNCl** and **$FcNBr_2$** are greater than most of the inorganic species[30] and as good as reported redox-active organic molecules applied in ARFBs.[9,11−14] Thus, the fast electrochemical kinetic results further indicate that **FcNCl** and **$FcNBr_2$** are suitable candidates for AORFBs. All electrochemical data of **FcNCl** and **$FcNBr_2$** are summarized in Table 1.

Paired with methyl viologen (**MV**, −0.45 V vs NHE, 3.5 M solubility in water), an established anolyte material for AORFBs,[12,15] the resulting **FcNCl**/**MV** and **FcN_2Br_2**/**MV** AORFB can deliver 1.05 V cell voltage (Figure 2). Together with their high charge capacities in 2.0 M NaCl, **FcNCl**/**MV** and **FcN_2Br_2**/**MV** AORFBs possess a theoretical energy density of 45.5 and 35.8 Wh/L, respectively (calculated using eq 3 given in the Experimental Section). The energy density of the **FcNCl**/**MV** AORFB is the highest energy density known to date for AORFBs and higher than state of the art vanadium ARFBs (41.8 Wh/L) and relatively less than Zn−Br_2 RFBs (ca. 65 Wh/L).[3,31,32] The theoretical energy densities can be higher when using a lower concentration NaCl supporting electrolyte, while the current performance of the AORFBs can be compromised due to less conductive ferrocene electrolyte. When dissolved in a NaCl supporting electrolyte, resulting **FcNCl** (Figure 3D) and **FcN_2Br_2** (Figure S6) catholytes are highly conductive. The data revealed that **FcNCl** exhibited

Table 1. Solubility, Capacity, and Electrochemical Data of FcNCl and FcN_2Br_2 RT

	solubility, M (capacity, Ah/L)				
compound	water	2.0 M NaCl	$E_{1/2}$, V (NHE)	D, cm^2/s	k^0, cm/s
FcNCl	4.0 (107.2)	3.0 (80.4)	0.61	3.74×10^{-6}	3.66×10^{-5}
FcN_2Br_2	3.1 (83.1)	2.0 (53.6)	0.61	3.64×10^{-6}	4.60×10^{-6}

DOI: 10.1021/jacs.6b10984
J. Am. Chem. Soc. 2017, 139, 1207−1214

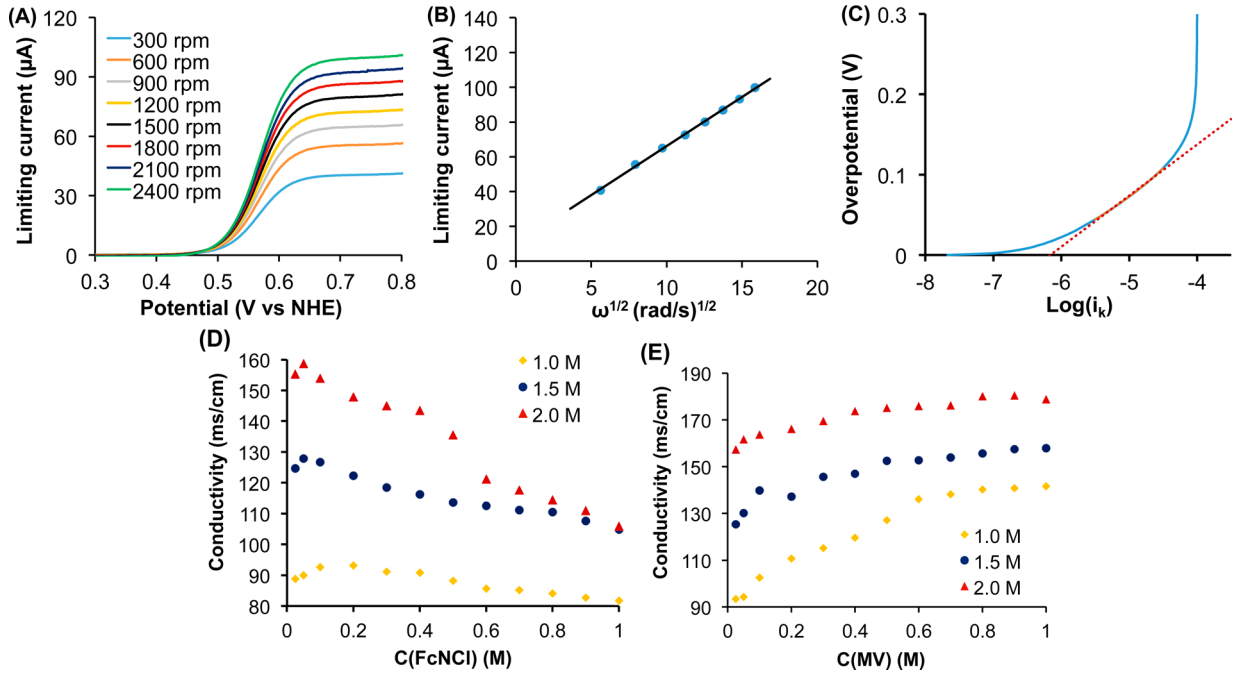

Figure 3. (A) Linear sweep voltammograms of **FcNCl** (1.0 mM in 0.5 M NaCl); (B) Levich plots of the limiting current vs the square root of rotation rates for **FcNCl**; (C) plot of overpotential over the logarithm of kinetic current and the corresponding fitted Tafel plot at 2400 rpm for **FcNCl**. (D and E) Conductivity measurements of **FcNCl** and **MV** from 0.05 to 1.0 M in NaCl solution at different concentrations, 1.0 (orange diamond trace), 1.5 (blue circle trace), and 2.0 M (red triangle trace) at RT.

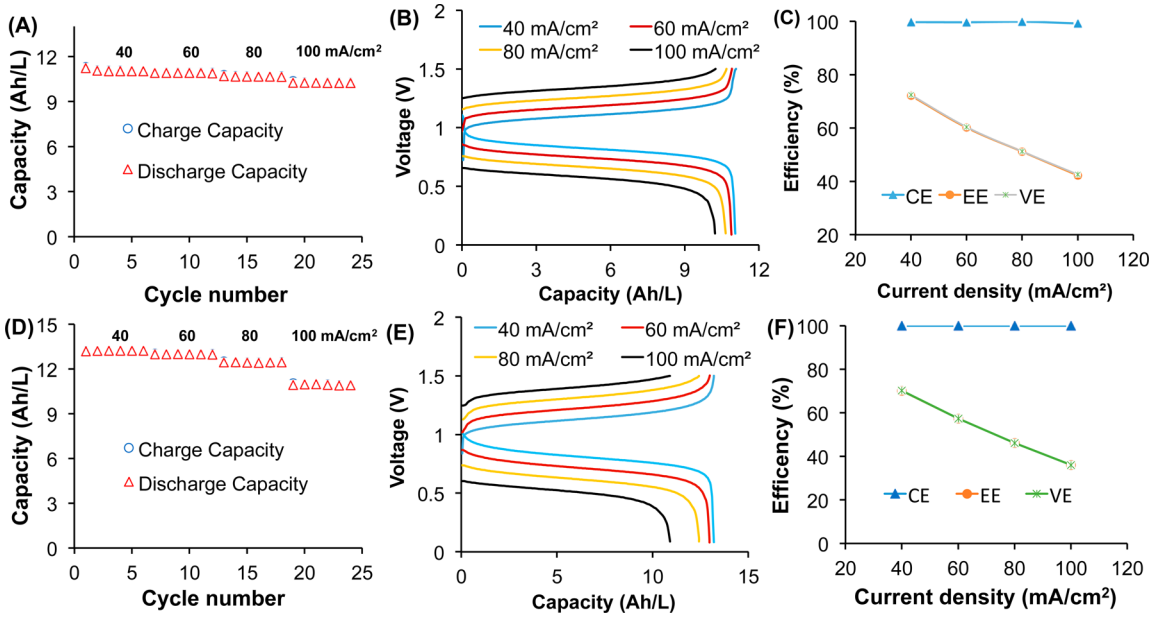

Figure 4. Capacity vs cycling numbers from 40 to 100 mA/cm^2 for the **FcNCl**/**MV** AORFB (A) and the **FcN_2Br_2**/**MV** AORFB (D). Representative charge and discharge profiles of the **FcNCl**/**MV** AORFB (B) and **FcN_2Br_2**/**MV** AORFB (E) from 40 to 100 mA/cm^2. Plots of averaged Coulombic efficiency (blue triangle), energy efficiency (orange circle), and voltage efficiency (green cross) versus current density of the **FcNCl**/**MV** AORFB (C) and **FcN_2Br_2**/**MV** AORFB (F). Conditions: catholyte, 0.5 M **FcNCl** (or **FcN_2Br_2**) in 2.0 M NaCl aqueous solution; anolyte, 0.5 M **MV** in 2.0 M NaCl aqueous solution; AMV anion-exchange membrane.

higher conductivities than **FcN_2Br_2**. Conductivity of both catholytes was boosted with increased NaCl concentrations from 1.0 to 2.0 M. In 2.0 M NaCl, both catholytes displayed exceptionally high conductivities above 105 mS/cm when tested at different concentrations. It is worth noting that such high conductivity is desired in order to achieve high current performance and high energy efficiency for RFBs. The decreased conductivities of **FcNCl** at higher concentrations are believed to be due to increased viscosities. Similar tests revealed a high conductivity for the **MV** anolyte, >150 mS/cm in 2.0 M NaCl (Figure 3E).

The **FcNCl**/**MV** AORFB cell design is outlined in Figure 1. Because of the cation nature of the redox-active species, **FcNCl** (or **FcN_2Br_2**) and **MV**, an anion-exchange membrane

DOI: 10.1021/jacs.6b10984
J. Am. Chem. Soc. 2017, 139, 1207−1214

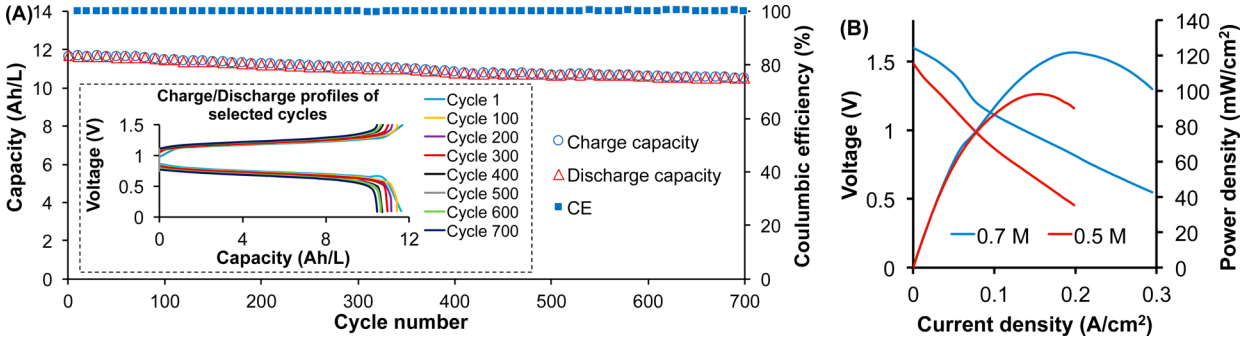

Figure 5. (A) Extended 700 cycle testing data of the 0.5 M **FcNCl**/**MV** AORFB at 60 mA/cm^2: capacity and Coulombic efficiency vs cycling numbers (for clarity, data points with an increment of 10 cycles were used for plotting); (inset) representative charge and discharge profiles of selected cycles. (B) Polarization and power density curves of the **FcNCl**/**MV** AORFB at 0.5 (red traces) and 0.7 M (blue traces) after full charge using 10 mA/cm^2.

(Selemion AMV) incorporated with pendant ammonium cation functionality was employed to allow selective Cl^- transport while suppressing the crossover of the positively charged active materials. Demonstration of the flow cell tests was conducted at 0.5 M for **FcNCl** in 2.0 M NaCl electrolyte (corresponding to 7.0 Wh/L energy density) with **MV** anolyte at RT. The current rate performance was investigated from 40 to 100 mA/cm^2 with increments of 20 mA/cm^2 (Figure 4A). Stable capacity retention was observed for 6 continuous cycles at each current density. Upon increasing current density from 40 to 60, 80, and 100 mA/cm^2, capacity retention stayed at 99%, 98%, and 95%, respectively, indicating a low cell resistance. For each current density, six charge and discharge cycles were tested with cutoff voltages at 1.5 V for the charge process and 0.1 V for the discharge process. Representative charge/discharges profiles of the **FcNCl**/**MV** AORFB are shown in Figure 4B. With the increase of the current density, the cell capacity only slightly decreased, which is benefitted from the high conductivity of electrolytes. Upon charging, both electrolyte solutions underwent immediate color changes, from red-orange to deep green for **FcNCl** and from colorless to deep purple for **MV** (see Figure 1). The observed color changes were consistent with the UV−vis spectra of **FcNCl** and **MV** in their charged and discharged states (Figure S7). **FcNCl** as the discharged state, exhibits absorbance at 440 nm, and its charged state, **FcNCl$_2$**, shows major absorption at 630 nm. The discharged state (**MV^{2+}**) of **MV** has no absorption in the visible region, while its charged state (**MV$^+$**) exhibits strong waves at 400 and 600 nm.

The trend of Coulombic efficiency, voltage efficiency, and energy efficiency of the 0.5 M FcNCl/MV AORFB are outlined in Figure 4C. Coulombic efficiency stayed above 99% at all current densities. Voltage efficiency and energy efficiency overlapped and decreased from 72% for 40 mA/cm^2 to 43% for 100 mA/cm^2. The observed trends for the voltage efficiency and the energy efficiency are typical and ascribed to the increased cell overpotential at higher current densities. The current performance of the neutral **FcNCl**/**MV** AORFB is outstanding as it is comparable with acidic vanadium RFBs and outperforms Zn−-halide RFBs.[3,31,32] Consistent with the high current performance, electrochemical impedance studies revealed a small area specific resistance of 2.9 Ω·cm^2 for the cell (see its Nyquist plot in Figure S8). The charge transfer resistance is only 0.29 Ω·cm^2, consistent with the fast electron transfer constants observed for **FcNCl** and **MV**. It is clear the ohmic resistance of the electrolytes and the membrane primarily contributed to the cell resistance.

Under similar conditions, the **FcN$_2$Br$_2$**/**MV** AORFB also exhibited stable cycling over four tested current densities (Figure 4D−F). Compared to the **FcNCl**/**MV** AORFB, the **FcN$_2$Br$_2$**/**MV** AORFB delivered relatively lower energy efficiencies, which is believed due to the lower conductivity of the **FcN$_2$Br$_2$** catholyte. For instance, the energy efficiency of the **FcN$_2$Br$_2$**/**MV** AORFB at 40 mA/cm^2 is 70%. It is believed that the observed differences in battery performance, and physical and chemical properties between **FcN$_2$Br$_2$** and **FcNCl** are attributed to their structural differences.

To further validate cycling performance, long cycling of the **FcNCl**/**MV** AORFB was examined at 60 mA/cm^2 (Figure 5A). The 0.5 M cell tested delivered rather stable capacity retention when tested for extended cycles. Even after 700 cycles, capacity still remained above 91%. The charge/discharge voltage profiles over time are provided in the Supporting Information (Figure S9). On average, the capacity retention was ca. 99.99% for a single charge/discharge cycle, which is equivalent to a capacity loss rate of 0.01% per cycle. The averaged energy efficiency stayed ca. 60% with small fluctuations over 700 cycles (Figure S10). The robust cycling performance is credited to excellent electrochemical and thermal stability of both active materials. For the same long cycling cell, the polarization curve was recorded at a full charge state using a small current density, 10 mA/cm^2. The resulting power density curve revealed a peak power density output at 100 mW/cm^2 (Figure 5B, red trace).

To demonstrate higher energy density performance, a flow cell was tested at 0.7 M (9.9 Wh/L energy density). The 0.7 M cell delivered an increased peak power density at 125 mW/cm^2 (Figure 5B, blue trace), which is in the same order of peak power density outputs observed for acidic and alkaline AORFBs.[7−11] In addition, the 0.7 M cell manifested stable capacity retention at 81% after 500 cycles (99.96% for a single charge/discharge cycle, Figure S11) and an increased energy efficiency at 65% at 60 mA/cm^2 (Figure S13). The improved power performance and energy efficiency of the 0.7 M cell are attributed to the decreased area specific resistance which was measured as 2.2 Ω·cm^2 in its Nyquist plot (Figure S14) compared to 2.9 Ω·cm^2 for the 0.5 M Cell. A small charge transfer resistance, 0.35 Ω·cm^2, was observed. The results indicated that the current and power performance of the **FcNCl**/**MV** AORFB can be further boosted by optimizing electrolyte conditions to reduce the cell ohmic resistance. The outstanding current and power performance highlights the practical potential of the **FcNCl**/**MV** AORFB to provide the

DOI: 10.1021/jacs.6b10984
J. Am. Chem. Soc. 2017, 139, 1207−1214

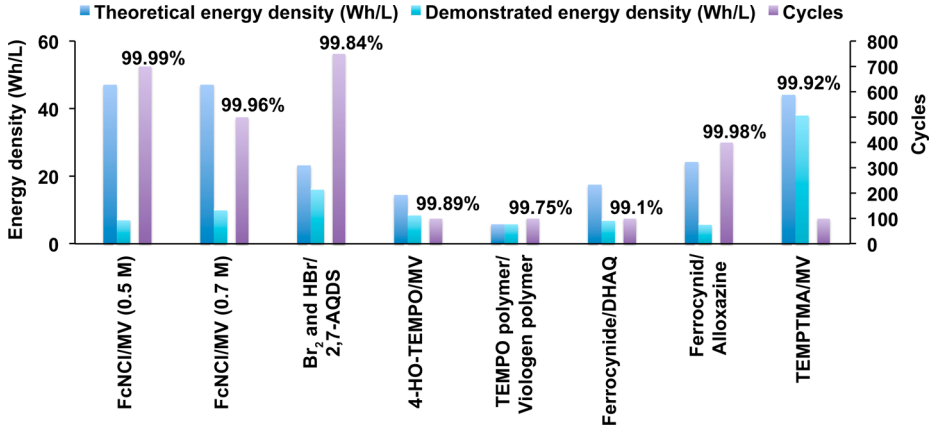

Figure 6. Bar chart comparison of theoretical energy density, demonstrated energy density, and tested cycles labeled with capacity retention per cycle of the **FcNCl/MV** AORFB and reported representative AORFBs. Chemical abbreviations: 2,6-AQDS, anthraquinon-2,6-disulfonic acid; DHAQ, 2,6-dihydroxyanthraquinone; alloxazine, alloxazine 7/8-carboxylic acid; TEMPTMA, *N,N,N*,2,2,6,6-heptamethylpiperidinyloxy-4-ammonium chloride.

necessary response to energy demands when coupled to electricity grids.

Postcell analysis for the **FcNCl/MV** AORFB after 700 cycles was conducted using cyclic voltammetry and ^{1}H NMR (Figures S13−15). Both CV and ^{1}H NMR studies indicated that there was no chemical degradation for either the catholyte or the anolyte. The postanalysis studies also indicated that there was no crossover between the catholyte and the anolyte as no **FcNCl** was detected in the ^{1}H NMR spectrum and CV of the **MV** anolyte and vice versa, highlighting the excellent compatibility of both catholyte and anolyte with the AMV membrane. Identical results were obtained for the 0.7 M cell after 500 cycles. Ongoing studies are aimed at elucidating the slow capacity decay and identifying optimal conditions to realize the full energy density of the **FcNCl/MV** AORFB, which warrants further studies of the system but is beyond the scope of this work.

Figure 6 provides a comparison of energy density (theoretical and demonstrated) and demonstrated cycles (labeled with cycling stability) of the **FcNCl/MV** AORFB and representative AORFBs reported to date.[11−14,33] More detailed technical comparison of AORFBs is provided in the Supporting Information (Table S1). It is clear that the **FcNCl/MV** AORFB has the highest theoretical energy density reported for AORFBs and represents one of the most stable cycling AORFBs. Notably, the neutral TEMPTMA/**MV** AORFB was demonstrated at 38 Wh/L for 100 cycles at ca. 99.93% capacity retention per cycle (TEMPTMA = *N,N,N*,2,2,6,6-heptamethylpiperidinyloxy-4-ammonium chloride).[15] In spite of a relatively complicated synthesis of TEMPTMA involving a precious Pd catalyst, the TEMPTMA/**MV** AORFB is a substantial advancement of our previous 4-OH-TEMPO/**MV** system[12] and highlights the importance of molecular engineering to improve the battery performance of AORFBs. In addition, the **FcNCl/MV** AORFB utilizes cheap noncorrosive NaCl electrolyte, and a low-cost AMV anion-exchange membrane ($50/m^2 vs $500/m^2 for Nafion cation-exchange membrane).[12] Compared to acidic/alkaline aqueous RFBs, these technical characteristics of the **FcNCl/MV** AORFB offer additional environment and safety benefits and cost advantages. The overall capital cost of the **FcNCl/MV** AORFBs for large-scale energy storage is estimated at $162/kWh compared to $447/kg for a VRFB Gen2 system (see Supporting Information for cost estimation).[34] One trade-off of the neutral **FcNCl/MV** AORFBs is the relatively lower current performance compared to acidic or alkaline AORFBs (Table S1) but this is still high enough for energy storage applications. Thus, when choosing a RFB technology for specific applications, one should consider overall technical features and make a balance between technical strengths and limitations.

It is worth noting that the redox potentials of both active materials, **FcNCl** (or **FcN_2Br_2**) and **MV**, are bracketed within the water-splitting voltage window (Figure 2, 1.5 V vs NHE for O_2 evolution reaction, [OER], and −1.0 V vs NHE for H_2 evolution reaction, [HER]), indicating that the OER and HER side reactions are not accessible within the cycling voltage window of the **FcNCl/MV** AORFB. Because of large overpotential of the OER and the HER on the carbon electrode, the observed water-splitting window, 2.5 V, is much wider than the standard thermodynamic free energy for water splitting, 1.23 V. The 2.5 V water splitting window allows developing high-voltage AORFBs. Voltage modulation can be achieved by synthetic tuning of redox potentials of organic materials and is expected to further enhance the energy density of AORFB. Regarding **FcNCl** and **FcN_2Br_2**, the second cyclopentadienide ligand can be also modified by an electron-withdrawing group to further increase the oxidation potential of the $Fe^{3+/2+}$ couple. Synthesis of new water-soluble ferrocene molecules is an ongoing effort in our research group.

CONCLUSIONS

In summary, we developed a new AORFB technology employing sustainable and tunable active electrolyte materials based on earth-abundant elements: C, H, N, and Fe. The synthesis of the new **FcNCl** and **FcN_2Br_2** cathode materials is convenient and scalable using commercial precursors, and their performance can be further improved through structural modification. Together with inexpensive, noncorrosive, and nonflammable NaCl supporting electrolyte, and a low-cost AMV membrane, the present high energy density and long cycling AORFB technology is economically attractive and environmentally friendly. Broadly, this work highlights the great potential of rationally designed redox-active organic molecules to construct low-cost, safe, and high-performance AORFBs by overcoming the technical constraints of traditional inorganic ARFBs, including resource limits, corrosive electrolytes, and membrane cost.

DOI: 10.1021/jacs.6b10984
J. Am. Chem. Soc. 2017, 139, 1207−1214

EXPERIMENTAL SECTION

Chemicals and Manipulations. All chemicals were purchased from Aldrich or TCI, stored in an argon glovebox, and used directly. Deionized water was purged overnight using N_2 before use. All experimental operations were conducted under a N_2 atmosphere. Conductivity of the electrolyte solutions was measured using a Mettler Toledo conductivity meter at RT. NMR studies were conducted using a Bruker 500 MHz NMR spectrometer. UV−vis data were collected using an Ocean Optics spectrometer. Elemental analysis was done at Atlantic Microlab.

Synthesis of (Ferrocenylmethyl)trimethylammonium Chloride (FcNCl). A 250 mL Schlenk flask was degassed with N_2 and maintained under N_2. (Ferrocenylmethyl)dimethylamine (20 g, 82.3 mmol) and methyl chloride (1 M in *tert*-butylether, 82.3 mL for 82.3 mmol, used 90 mL) were combined in 50 mL of CH_3CN in a 250 mL flask. The reaction mixture was stirred at RT overnight. The red-orange precipitate was formed and collected by filtration. A 100 mL amount of ether was added to the supernatant solution to precipitate a second crop of the product. The combined product was washed twice with 40 mL of ether and dried under vacuum. The product is hydroscopic and stored in a dry desiccator. The yield was ca. 95% (23.0 g). ^{1}H NMR (D_2O, 300 MHz): δ (in ppm), 2.91 (s, 9 H), 4.24 (s, 5 H), 4.35 (s, 2H), 4.39 (s, 2H), 4.47 (d, 2H). Anal. Calcd for $C_{14}H_{20}NClFe{\cdot}0.5\ H_2O$: C, 55.53; H, 6.94; N, 4.63. Found C, 55.26; H, 7.05; N, 4.61.

Synthesis of N^1-Ferrocenylmethyl-N^1,N^1,N^2,N^2,N^2-pentamethylpropane-1,2-diaminium dibromide (FcN_2Br_2). FcN_2Br_2 was synthesized from (ferrocenylmethyl)dimethylamine (3.4 g, 14 mmol) and (3-bromopropyl)trimethylammonium bromide (3.8 g, 14.5 mmol) in 20 mL CH_3CN and 10 mL of DMSO in a procedure similar as **FcNCl**. The yield was 90.1% (6.2 g). ^{1}H NMR (D_2O) δ (in ppm), 2.25 (m, 2 H), 2.94 (s, 6 H), 3.12 (s, 9 H), 3.19 (t, 2 H), 3.31 (t, 2 H), 4.26 (s, 5 H), 4.42 (d, 2 H), 4.46 (s, 2 H), 4.48 (s, 2H).

Solubility Tests. Solubility of **FcNCl**, FcN_2Br_2, **FcN**, and **MV** was measured in water or 2.0 M NaCl by preparing a 1.0 mL supersaturated solution in a 5.0 mL graduated cylinder. Similar solubility tests in water were conducted for ferrocenecarboxylic acid, 1,1′-ferrocenedicarboxylic acid, ferrocenecarboxylic acid, and 1,1′-ferrocenedimethanol.

Electrochemical CV Studies. All electrochemical CV experiments were carried out in 0.5 M NaCl electrolyte solutions. Cyclic voltammetry experiments were performed with a Gamry 1000E potentiostat. All potentials were referenced to NHE according to the known $MV^{2+/1+}$ redox couple (−0.45 V vs NHE).[35] The working electrode (1 mm PEEK-encased glassy carbon, Cypress Systems EE040) was polished using Al_2O_3 (BAS CF-1050, dried at 150 °C under vacuum) suspended in deionized H_2O, then rinsed with deionized H_2O, and dried with an air flow. The reference electrode consisted of a silver wire coated with a layer of AgCl and suspended in a solution of 0.5 M NaCl electrolyte. A glassy carbon rod (Structure Probe, Inc.) was used as the counter electrode.

Electrochemical RDE Studies. All linear sweep voltammetry (LSV) studies were conducted using a Gamry 1000E potentiostat in a three-electrode configuration, a glassy carbon disk working electrode (5 mm Teflon-encased glassy carbon disk, Pine Research Instrumentation) along with a glassy carbon counter electrode, and a Ag/AgCl reference electrode as used in CV studies. Before data collection, the disk electrode was prepared using the procedure described in the CV studies. The electrode was then rotated from 300 to 2400 rpm with increments of 300 rpm, which was controlled by a Pine MSR rotator system. LSV scans were recorded at a rate of 5 mV/s from 0.3 to 0.8 V vs NHE. At each rotation rate, the LSV were recorded three times to ensure repeatability. The limiting currents (i.e., the mass transport-limited current intensity) were taken at 0.7 V vs NHE for **FcNCl** and plotted over the square root of the rotation rate (rad/s). The data were fitted to yield a straight Levich plot, with the slope defined by the Levich equation (eq 1 below), where n = 1 for a one-electron process, Faraday's constant F = 96485 C/mol, electrode area A = 0.196 cm^2, **FcNCl** concentration C_O = 1.0 mM, D is the diffusion coefficient, and kinematic viscosity n = 0.009 cm^2/s for 0.5 M NaCl solution. The calculations yielded the diffusion coefficients of **FcNCl** as 3.25 × 10^{-6} cm^2/s. A plot of overpotential versus $\log_{10}(i_k)$ was constructed for the LSV data collected at 2400 rpm for **FcNCl** where i_k is the kinetic current for the oxidation of **FcNCl**. The X intercept of the fitted Tafel plot gives the log of the exchange current i_0 (0.7 μA), which equals FAC_Ok^0 (eq 2), and gives an electron transfer rate constant k^0 = 2.29 × 10^{-5} cm/s for **FcNCl**. Under the same conditions, LSV studies of FcN_2Br_2 yielded a diffusion coefficient of 3.64 × 10^{-6} cm^2/s and an electron transfer rate constant of 4.60 × 10^{-6} cm/s.

$$\text{Levich plot slope} = 0.620nFAC_OD^{2/3}\nu^{-1/6} \quad (1)$$

$$i_0 = FAC_Ok^0 \quad (2)$$

Flow Cell Tests. The flow cells for the **FcNCl**/**MV** AORFB and the FcN_2Br_2/**MV** AORFB were constructed with two carbon electrolyte chambers, two graphite felt electrodes (SGL Carbon Group, Germany), a piece of anion-exchange membrane (AMV, 120 μm thickness, pore size < 10 Å, Selemion, Japan) sandwiched between graphite felts, and two copper current collectors. Each carbon chamber was connected with an electrolyte reservoir using a piece of Viton tubing. The electrolyte reservoir is home designed and is a 10 mL glass tube (2 cm inner diameter). The active area of the cell was 10 cm^2. A Masterflex *L/S* peristaltic pump (Cole-Parmer, Vernon Hills, IL) was used to press the Viton tubing to circulate the electrolytes through the electrodes at a flow rate of 60 mL/min. In each reservoir, the balanced flow cell employed 11−13 mL of the NaCl electrolytes containing 0.5 or 0.7 M active materials. Both reservoirs were purged with nitrogen to remove O_2 and then sealed before cell cycling. The flow cell was galvanostatically charged/discharged at RT on a battery tester (Land Instruments) in the voltage range of 1.5−0.1 V at current densities ranging from 40 to 100 mA/cm^2. The polarization curve and electrochemical impedance spectra were recorded using a Gamry 1000E potentiostat. The discharged and charged states of **FcNCl** and **MV** were measured using UV−vis spectroscopy. Postcell studies of the **FcNCl**/**MV** AORFB using ^{1}H NMR and CV were conducted for both electrolytes at the end of the cell tests (Figures S15−17).

Calculation of Theoretical Energy Density. The theoretical energy density of the **FcNCl**/**MV** AORFB was calculated using eq 3, where n is the number of electrons involved into the cell reaction, C is the lower concentration of two electrolytes, F is Faraday's constant, 26.8 Ah/mol, V is the cell voltage, and v represents the factor of overall volumes of anolyte and catholyte

$$\text{energy density(Wh/L)} = nCFV/\mu_v \quad (3)$$

μ_v is the volume factor; μ_v = 1 + lower electrolyte concentration/higher electrolyte concentration. When two electrolytes have an equal concentration, μ_v is 2. Concentrations of 3.0 M for **FcNCl** and 2.0 M for FcN_2Br_2 in 2.0 M NaCl were used for calculation; 3.5 M **MV** in water was used for calculation as **MV** has a high conductivity (130 mS/cm) without additional supporting electrolyte.

For the **FcNCl**/**MV** AORFB, μ_v = 1 + [**FeNLc**]/[**MV**] = 1 + 3/3.5 = 1.86; then its energy density = (1 × 3.0 × 26.8 × 1.05)/1.86 = 45.5 Wh/L.

For the FcN_2Br_2/**MV** AORFB, μ_v = 1 + [FeN_2Br_2]/[**MV**] = 1 + 2/3.5 = 1.86; then its energy density = (1 × 2 × 26.8 × 1.05)/1.57 = 35.8 Wh/L.

ASSOCIATED CONTENT

Supporting Information

The Supporting Information is available free of charge on the ACS Publications website at DOI: 10.1021/jacs.6b10984.

Cyclic votammograms of **FcNCl**, plot of i_c and i_a over the square root of scan rates for **FcNCl**, cyclic votammograms of FcN_2Br_2, plot of i_c and i_a over the square root of scan rates for FcN_2Br_2, linear sweep voltammograms of FcN_2Br_2, Levich plot of the limiting current vs the square root of rotation rates for FcN_2Br_2, plot of overpotential

DOI: 10.1021/jacs.6b10984
J. Am. Chem. Soc. 2017, 139, 1207−1214

over the logarithm of kinetic current and the corresponding fitted Tafel plot for **FcN_2Br_2**, conductivity measurements of **FcN_2Br_2**, UV−vis spectra, Nyquist plot of the 0.5 M **FcNCl**/**MV** AORFB before cycling, representative charge/discharge voltage profiles, extended 500 cycle test data, plot of energy efficiency vs cycling numbers, postcell CV studies, postcell ^{1}H NMR studies, comparison of the ^{1}H NMR spectra, cyclic voltammogram of combined **FcNCl** and **MV**, summary of technical characters of the reported AORFBs at extended cycles, cost estimation of the **FcNCl**/**MV** AORFB (PDF)

AUTHOR INFORMATION

Corresponding Author

*Leo.Liu@usu.edu

ORCID

T. Leo Liu: 0000-0002-3698-1096

Notes

The authors declare no competing financial interest.

ACKNOWLEDGMENTS

We thank Utah State University for providing faculty startup funds to the PI (Tianbiao Liu) and the Utah Science Technology and Research initiative (USTAR) program for supporting the investigation of new organic redox-active compounds and their applications in redox flow batteries. B.H. and C.D.B. are grateful for their scholarships sponsored by the China CSC abroad studying program and USU Presidential Doctoral Research Fellowship (PDRF) program, respectively. Z.R. is thankful for the 2016 Summer Research Award offered by the College of Science at USU to conduct undergraduate research in the Liu lab.

REFERENCES

(1) Dunn, B.; Kamath, H.; Tarascon, J.-M. *Science* **2011**, *334*, 928.
(2) Yang, Z.; Zhang, J.; Kintner-Meyer, M. C. W.; Lu, X.; Choi, D.; Lemmon, J. P.; Liu, J. *Chem. Rev.* **2011**, *111*, 3577.
(3) Soloveichik, G. L. *Chem. Rev.* **2015**, *115*, 11533.
(4) Darling, R. M.; Gallagher, K. G.; Kowalski, J. A.; Ha, S.; Brushett, F. R. *Energy Environ. Sci.* **2014**, *7*, 3459.
(5) *ARPA-E GRIDS Program Overview*; DOE Office of ARPR-E, 2011; https://arpa-e.energy.gov/?q=arpa-e-programs/grids.
(6) *Program Planning Document on Energy Storage*; DOE Office of Electricity Delivery&Energy Reliability, 2011; http://energy.gov/oe/downloads/energy-storage-program-planning-document-2011.
(7) Xu, Y.; Wen, Y.; Cheng, J.; Yanga, Y.; Xie, Z.; Cao, G. In *World Non-Grid-Connected Wind Power and Energy Conference, 2009*; WNWEC 2009; IEEE: Nanjing, China, 2009; p 1.
(8) Xu, Y.; Wen, Y.-H.; Cheng, J.; Cao, G.-P.; Yang, Y.-S. *Electrochim. Acta* **2010**, *55*, 715.
(9) Huskinson, B.; Marshak, M. P.; Suh, C.; Er, S.; Gerhardt, M. R.; Galvin, C. J.; Chen, X.; Aspuru-Guzik, A.; Gordon, R. G.; Aziz, M. J. *Nature* **2014**, *505*, 195.
(10) Yang, B.; Hoober-Burkhardt, L.; Wang, F.; Surya Prakash, G. K.; Narayanan, S. R. *J. Electrochem. Soc.* **2014**, *161*, A1371.
(11) Lin, K.; Chen, Q.; Gerhardt, M. R.; Tong, L.; Kim, S. B.; Eisenach, L.; Valle, A. W.; Hardee, D.; Gordon, R. G.; Aziz, M. J.; Marshak, M. P. *Science* **2015**, *349*, 1529.
(12) Liu, T.; Wei, X.; Nie, Z.; Sprenkle, V.; Wang, W. *Adv. Energy Mater.* **2016**, *6*, 1501449.
(13) Janoschka, T.; Martin, N.; Martin, U.; Friebe, C.; Morgenstern, S.; Hiller, H.; Hager, M. D.; Schubert, U. S. *Nature* **2015**, *527*, 78.
(14) Lin, K.; Gómez-Bombarelli, R.; Beh, E. S.; Tong, L.; Chen, Q.; Valle, A.; Aspuru-Guzik, A.; Aziz, M. J.; Gordon, R. G. *Nat. Energy* **2016**, *1*, 16102.
(15) Janoschka, T.; Martin, N.; Hager, M. D.; Schubert, U. S. *Angew. Chem., Int. Ed.* **2016**, *55*, 14427.
(16) Wei, X.; Xu, W.; Vijayakumar, M.; Cosimbescu, L.; Liu, T.; Sprenkle, V.; Wang, W. *Adv. Mater.* **2014**, *26*, 7649.
(17) Wei, X.; Xu, W.; Huang, J.; Zhang, L.; Walter, E.; Lawrence, C.; Vijayakumar, M.; Henderson, W. A.; Liu, T.; Cosimbescu, L.; Li, B.; Sprenkle, V.; Wang, W. *Angew. Chem., Int. Ed.* **2015**, *54*, 8684.
(18) Duan, W.; Vemuri, R. S.; Milshtein, J. D.; Laramie, S.; Dmello, R. D.; Huang, J.; Zhang, L.; Hu, D.; Vijayakumar, M.; Wang, W.; Liu, J.; Darling, R. M.; Thompson, L.; Smith, K.; Moore, J. S.; Brushett, F. R.; Wei, X. *J. Mater. Chem. A* **2016**, *4*, 5448.
(19) Nagarjuna, G.; Hui, J.; Cheng, K. J.; Lichtenstein, T.; Shen, M.; Moore, J. S.; Rodríguez-López, J. *J. Am. Chem. Soc.* **2014**, *136*, 16309.
(20) Huang, Q.; Yang, J.; Ng, C. B.; Jia, C.; Wang, Q. *Energy Environ. Sci.* **2016**, *9*, 917.
(21) Zhao, Y.; Ding, Y.; Song, J.; Li, G.; Dong, G.; Goodenough, J. B.; Yu, G. *Angew. Chem., Int. Ed.* **2014**, *53*, 11036.
(22) Ding, Y.; Yu, G. *Angew. Chem., Int. Ed.* **2016**, *55*, 4614.
(23) Brushett, F. R.; Vaughey, J. T.; Jansen, A. N. *Adv. Energy Mater.* **2012**, *2*, 1390.
(24) Kealy, T. J.; Pauson, P. L. *Nature* **1951**, *168*, 1039.
(25) Wilkinson, G.; Rosenblum, M.; Whiting, M. C.; Woodward, R. B. *J. Am. Chem. Soc.* **1952**, *74*, 2125.
(26) Fischer, E. O.; Pfab, W. *Z. Naturforsch.* **1952**, *B7*, 377.
(27) Wei, X.; Cosimbescu, L.; Xu, W.; Hu, J. Z.; Vijayakumar, M.; Feng, J.; Hu, M. Y.; Deng, X.; Xiao, J.; Liu, J.; Sprenkle, V.; Wang, W. *Adv. Energy Mater.* **2015**, *5*, 1400678.
(28) Lindsay, J. K.; Hauser, C. R. *J. Org. Chem.* **1957**, *22*, 355.
(29) Nielson, R. M.; Hupp, J. T. *Inorg. Chem.* **1996**, *35*, 1402.
(30) Shah, A. A.; Watt-Smith, M. J.; Walsh, F. C. *Electrochim. Acta* **2008**, *53*, 8087.
(31) Leung, P.; Li, X.; Ponce de Leon, C.; Berlouis, L.; Low, C. T. J.; Walsh, F. C. *RSC Adv.* **2012**, *2*, 10125.
(32) Li, L.; Kim, S.; Wang, W.; Vijayakumar, M.; Nie, Z.; Chen, B.; Zhang, J.; Xia, G.; Hu, J.; Graff, G.; Liu, J.; Yang, Z. *Adv. Energy Mater.* **2011**, *1*, 394.
(33) Huskinson, B.; Marshak, M. P.; Gerhardt, M. R.; Aziz, M. J. *ECS Trans.* **2014**, *61*, 27.
(34) Viswanathan, V.; Crawford, A.; Stephenson, D.; Kim, S.; Wang, W.; Li, B.; Coffey, G.; Thomsen, E.; Graff, G.; Balducci, P.; Kintner-Meyer, M.; Sprenkle, V. *J. Power Sources* **2014**, *247*, 1040.
(35) Bird, C. L.; Kuhn, A. T. *Chem. Soc. Rev.* **1981**, *10*, 49.

DOI: 10.1021/jacs.6b10984
J. Am. Chem. Soc. 2017, 139, 1207−1214